Journal of Bio- and Tribo-Corrosion (2022) 8:97
https://doi.org/10.1007/s40735-022-00691-z

Crispy Dry Chili Extract as an Eco-Friendly Corrosion Inhibitor for Mild Steel in Chloride Solutions: Experimental and Theoretical Studies

Omnia S. Shehata[1] · Amr H. Abdel Fatah[2] · Hazem Abdelsalm[3] · Amal M. Abdel-Karim[1]

Received: 3 April 2022 / Revised: 14 July 2022 / Accepted: 24 July 2022

Abstract

The development of eco-friendly corrosion inhibitors is an area under several investigations; especially, natural plant extract. Such as crispy dry capsicum chili extracts (containing capsaicinoids as the active ingredient), the plant extract is an inexpensive and renewable material. Surface properties were studied such as fourier transforms infrared spectroscopy, contact angle measurements (θ), and scanning electron microscope. The inhibitive effects of the extract on mild steel in chloride solutions were experimentally evaluated by electrochemical methods such as potentiodynamic polarization, and electrochemical impedance spectroscopy. The results illustrated that the maximum inhibition efficiency of the coating was 97.1, 94.7, and 85.2%, for mild steel in 3.5% NaCl, 2.0, and 1.0 M HCl, respectively. The protective hydrophobic film attributed high protection to the homogeneous distribution. The significance of quantum chemical descriptors to the performance of the extract as a corrosion inhibitor was determined using the density functional theory. Quantum parameters were evaluated and discussed, such as the highest and lowest occupied orbital energy, the energy gap, hardness, and other quantum descriptors.

Graphical Abstract

Keywords Plant extract · Eco-friendly corrosion inhibitor · PDP · Contact angle · DFT

1 Introduction

Hydrochloric acid is widely used in major industries related to ferrous materials, especially those related to mild steel. Water treatment, oil/gas exploration, oil well acidizing, and acid pickling chemical cleaning are among its applications. The mitigation of accelerating corrosion problems which incur huge costs by using carefully selected corrosion inhibitors. Today, environmentally friendly inhibitors are replacing toxic ones

✉ Amal M. Abdel-Karim
am.abdelkarim@nrc.sci.eg; amalabdelkarim720@gmail.com

[1] Physical Chemistry Department, National Research Centre, 33 El Bohouth St. Dokki, Giza P.O.12622, Egypt

[2] Faculty of Biotechnology, Modern Science and Arts University, 6 October City, Giza, Egypt

[3] Theoretical Physics Department, National Research Centre, 33 El Bohouth St. Dokki, Giza 12622, Egypt

Published online: 27 August 2022

[1–5]. Organic compounds extracted from plants are considerably effective inhibitors, as they contain hetero- atoms and ring structures. Thus, inhibitors derived from plant extracts are gaining attraction as eco-friendly, economic, renewable sources of corrosion inhibitors [6–8]. The chili pepper fruit contains a high concentration of capsaicinoids in addition to polar ascorbic acid molecules [9]. Therefore, it is considered a strong candidate for anticorrosion studies. Capsaicinoids are easily extracted from hot peppers in organic solvents using a low-cost technique with a high yield. Capsaicinoids are the class of compounds found in members of the capsicum family (peppers). Capsaicinoids are structurally divided into a vanillyl moiety, secondary amide, and an unsaturated hydrophobic tail derived from a fatty acid [10–12]. In a previous study, the inhibition efficiency of capsaicinoids extracts on 304 stainless steel was 92.32% during 30 min immersion in 1.0 M HCl at room temperature [13]. The maximum inhibition efficiency of capsicum extract from green annuum fruit paste against mild steel corrosion in 1.0 M HCl, reached 85%. Here the inhibitor was added at concentrations of 500–1400 mg l^{-1} and the immersion time was five hours [14]. Capsaicinoids extracted from chili peppers in the concentration range (0.8–20 mg l^{-1}) also protect carbon steel from corrosion in NaCl solution; apparently, because the inhibitor molecules are adsorbed on the metal surface and thus block the active sites, preventing the aggressive media from reaching the metal surface [15]. In combined capsaicinoids with Poly acryl-amide, it is found that the inhibition efficiency is ascribed to the hydrophobic group of capsaicinoids which protect the mild steel surface immersed in 1.0 M HCl [16].

In the present study, we explore the corrosion protection in an aggressive medium for steels coated with a slimy film of capsicum after five days of immersion. This is through studying the effect of the capsaicinoids on different alloying elements such as mild and carbon steel in 1.0 M HCl, and on mild steel in different corrosive media 2.0 M HCl, and 3.5% NaCl. The inhibition efficiency was investigated using various techniques: open circuit potential (OCP), potentiodynamic polarization (PDP), and electrochemical impedance (EIS). The electronic structure and adsorption behavior of the slim coat of natural product extracted from crispy dry red chili was theoretically determined. The surface morphologies of the thin films were studied by scanning electron microscopy (SEM) and Fourier transform infrared spectroscopy (FTIR). The hydrophobic property was assessed from the contact angle measurements

2 Experimental

2.1 Materials

The solvents methanol, glacial acetic acid, distilled water, and acetonitrile (J.T. Baker, Phillips- burg, NJ, USA) utilized HPLC-grade. The bi-distilled water was obtained from a Milli-Q water bi-distillation system (Millipore, Bedford, MA, USA). The reference standards of, capsaicinoids and dihydrocapsaicin (more than 95% of purity) were obtained from Cayman Chemical Company (Arbor, MI, USA). All solvents used as mobile phase were filtered and degassed using Millipore filters (0.22 µm pore size, filter type GV (Durapore) PVDF for water, and FG (Fluoropore) PTFE for organic solvents). The electrolyte solutions 1.0 M and 2.0 M HCl were prepared from 37% hydrochloric acid. NaCl was purchased from Aldrich Chemical Co. Ltd.

The mild and Carbon steel substrates were cut into coupons with dimensions ($1.0\times3.0\times0.03$ cm^3) and then connected to the copper wire after isolation, leaving an appropriate cross-sectional area ($1.0\times1.0\times0.03$ cm^3). The chemical analyses of the working electrodes were listed in Table 1.

2.2 Extraction and Analysis of Capsaicinoids

Extraction of capsicum was done by acetone and hexane as follows: red chili procured in Egypt was dried at 50 °C for 2 hours to bring down the moisture to nearly 5%. The crisp dry chili was passed through a grinder with a suitable sieve to get a mixture of seeds and pericarp flakes. This mixture was passed through a smaller mesh sieve to get two parts, firstly big flakes of per carp free of seeds; secondly a mixture of smaller flakes and seeds. The Mixture (400 g) was loaded in a container and was extracted with a solvent mixture containing 60% of acetone, and 40% of hexane (V/V). Consequently, the solvent was added to the mixture to keep it soaked, with a contact time of 4 hours. Finally, a sample was added to Rota-evaporator to evaporate solvent at temperatures 56 °C and 68.8 °C for 30 min till all solvents were evaporated.

The analysis of the proximate phytochemical screening and constituents of the capsaicinoids was performed using an HPLC water, Model alliance e2695, and PDA detector Model 2998 as shown in Fig. 1.

The separation of capsaicinoids was achieved with a select column C18 (250* 4.6/5 um), and a mobile phase

Table 1 The chemical analysis of mild and carbon steel substrates

Alloy	C%	Mn%	P%	S%	Cu%	Si%	Ni%	Al%	Cr%	Ti%
Mild steel	0.047	0.29	0.017	0.013	0.054	0.037	0.057	0.003	0.034	0.02
Carbon steel	0.18	0.90	0.040	0.050	0.200	0.100	–	–	–	–

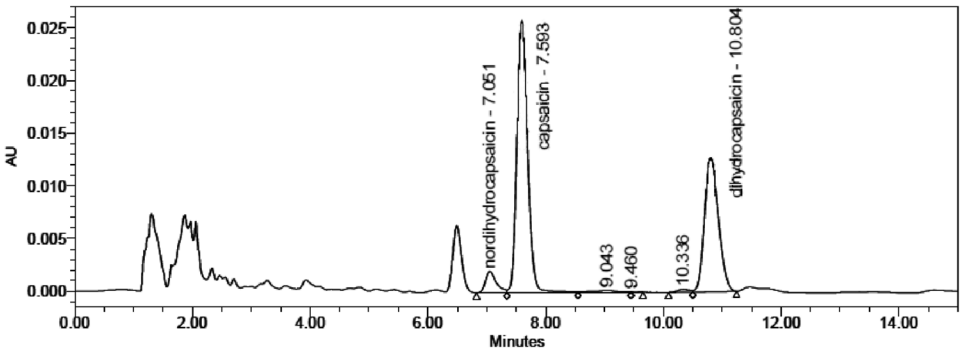

Fig. 1 Identification of capsaicin in a sample at 280 nm via PDA detector

Table 2 The active ingredients of the capsaicinoids

Capsaicinoids	%(SHU*)
Capsaicin	52.11
Dihydrocapsaicin	34.86
Nordihydrocapsaicin	13.03

*Scoville heat units

consisting of acetonitrile: 1% acetic acid 50:50 in isocratic mode at 1.5 ml min^{-1} of flow rate, column temperature 40 °C; injection volume 25 ul. Capsaicinoids in the sample were indicated by the relative retention time to standards, and by comparing the PDA spectra between standards, the active ingredient of capsaicinoids was detected in a sample at 280 nm and listed in Table 2.

2.3 Coating Process

The working electrodes were successively abraded with various grades of emery paper (up to 1200) to ensure the proper surface. Cleaning and degreasing were performed in analytical reagent-grade acetone, followed by rinsing with double distilled water before drying in air. The coating films were prepared after five days of immersion in dissolving extracted (1100 ppm) at room temperature, then removed and dried in air. The substrates became coated with a slim layer of capsicum. The coated substrates were tested in different aggressive solutions 1, 2 M HCl, and 3.5% NaCl to evaluate inhibition efficiencies.

2.4 Surface Morphology

To explore the surface morphologies, the uncoated and coated specimens of area 0.5 cm^2 were immersed in 1.0 M, 2.0 M HCl, and 3.5% NaCl, for three hours at room temperature. Top-view SEM images of the sample surfaces were collected using a Quanta 250 field emission gun with an accelerating voltage of 30 kV (FEI Company, Netherland). The nature of the protective film formed on the mild steel surface was determined from the FTIR spectra of the dried powder coating and the mild steel before and after coating. The FTIR spectra were obtained by a Perkin Elmer Spectrometer.

The surface wettability of the formed film was investigated in an OCA 15EC instrument (Data Physics Instrument Gmbh, Germany). A droplet of de-ionized water was mounted on the film surface through a micro-syringe. The curvature profile of the fixed-volume drop was created, and the contact angles were averaged from at least three individual measurements taken at different locations on the metal surface.

2.5 Electrochemical Techniques

The electrochemical measurements for the uncoated and coated working electrodes were tested in different corrosive media, for 30 min, until a steady-state potential was reached. The Work Station Metrohm autolab potentiostat/ galvanostat version PGSTAT 302 N was used. A three-electrode cell was used which include working electrodes connected with the reference electrode Ag/AgCl, and platinum wire as a counter electrode. AC impedance responses were recorded at open circuit potential (OCP), with a sinusoidal excitation signal of 10.0 mV peak-to-peak in the frequency range from 0.01 Hz to 100 kHz. Cell impedance (Z) and phase shift (θ) were included. Potentiodynamic polarization scans were conducted at a rate of 1.0 mV s^{-1} from cathode to anode directions in a potential range from – 1.4 V to 0.2 V. Data obtained were analyzed with software Nova 1.11. Three sets were repeated for various solutions to achieve accurate results at room temperature.

2.6 Computational Studies

All Quantum chemistry calculations and geometry optimization were performed using density functional theory (DFT). The energy of the highest occupied molecular orbital, E_{HOMO}, and the lowest unoccupied molecular orbital,

E_{LUMO} were utilized to show the adsorption capability of the organic compounds.

3 Result and Discussion

Capsaicinoids are the main constituent of the extract as seen in Fig. 1, and Table 1 Capsaicinoids are structurally divided into three main regions: (i) vanillyl moiety; (ii) secondary amide linker that connects both extremes of the molecule, and (iii) unsaturated hydrophobic tail derived from fatty acid as seen in Fig. 2

3.1 Contact Angle (θ)

The wetting phenomenon is strongly affected by the roughness of the metal surface, which itself is altered by the coating. The wettability of the metal surface is indexed by the contact angle between the liquid and the solid metal. As the metal surface was planar the contact angle can be geometrically measured. A contact angle higher than 70, indicates strong water repellence [17]. As shown in Fig. 3, the contact angle was 50° on the uncoated metal and 73° on the coated metal, implying that the coating decreased the wettability and increased the hydrophobic nature of the surface. The increased contact angle also indicates the increases of roughness of the metal surface [18]. The hydrophobic nature of the capsaicinoids coating improved the corrosion efficiency of the metal surface.

3.2 Fourier Transforms Infrared Spectroscopy (FTIR) Analysis

FTIR is widely employed in characterization owing to its non-destructive nature and is easily identified Fig. 4 shows the FTIR spectra at the range of 3600–400 cm^{-1} of the crisp dry red chili extracts as a powder and as a coating on the metal surface. The peaks at 3374 and 3350 cm^{-1}were the stretching vibrations of N–H and O–H groups, respectively [19]. The intense band in the 2945–2855 cm^{-1} range was ascribed to aliphatic C–H stretching of CH_2 and CH_3 [20], and the intense band around 1760 cm^{-1} was ascribed to overlapped signals of C=O and aromatic C=C stretching vibration. The small band around 1540 cm^{-1} was assigned to aromatic C–N stretching and N–H bending in amides. Following this peak, a small peak associated with amides and the stretching band at 1460 cm^{-1} represents C–C in

Fig. 2 Chemical structure of capsaicinoids

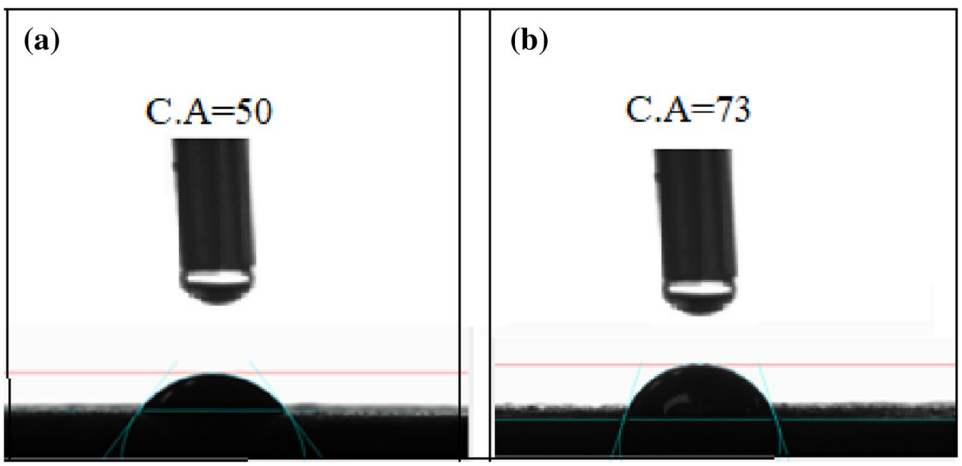

Fig. 3 The contact angles on mild steel surface **a** before coating and **b** after coating

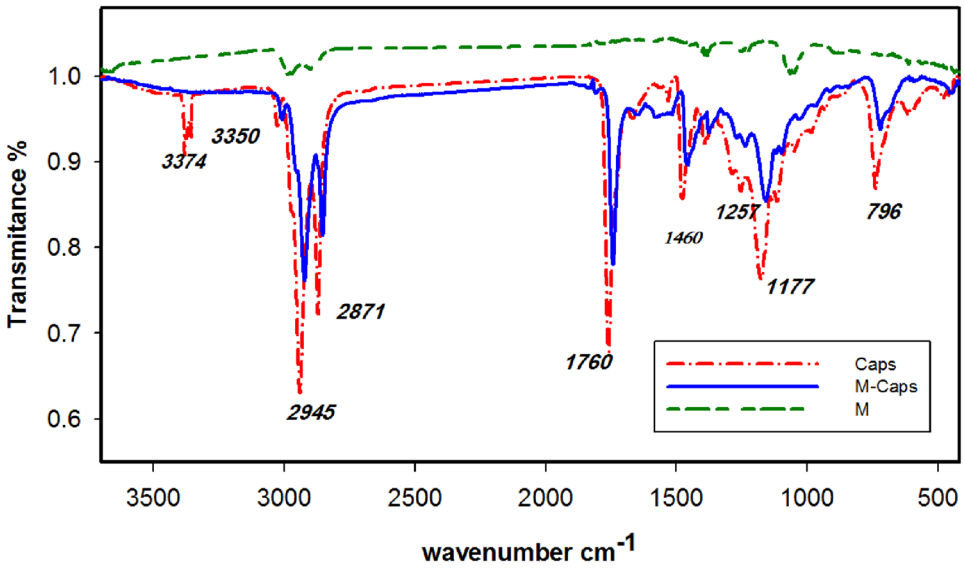

Fig. 4 FTIR spectra of the extracts crisp dry red chili (Caps) as powder and (M) uncoated, and (M-Caps) coated mild steel

aromatic rings [21]. Vibration bands after 1257 cm^{-1} and the stretching peak at 1177 cm^{-1} were associated with the C–O–C group of the aromatic rings of CH_2, OH, and C–O aliphatic groups. The band at 796 cm^{-1} represents C–H out-of-plane bending vibrations confirming the presence of an aromatic ring**.**

All bending and stretching peaks confirmed the chemical structure of capsaicinoids (as seen in Fig. 3. Comparing the spectra of the capsaicinoids coated on mild steel with those of pure capsaicinoids, it was observed that capsaicinoids delimit the adsorbed water on the steel surface. In particular, the intensity of the O–H stretching peak disappeared, while the intensities of the other peaks gradually decreased and shifted. This behavior was related to the major polar functional groups OH and NH at 2945 and 2871 cm^{-1}, respectively. When incorporated with Fe^{2+}, these bands shifted to 2920 and 2840 cm^{-1}, respectively. The stretching mode of the amide carbonyl group at 1760 cm^{-1} shifted to 1745 cm^{-1}. The shift in stretching frequencies of these functional groups confirmed the active compounds formed complexes with Fe^{2+} on the metal surface [22]**.**

3.3 Electrochemical Measurements

3.3.1 Open Circuit Potential (OCP)

Simple measurement OCP is shown in Fig. 5; it presents the potential-time plots of the coated (labeled 1) and uncoated (labeled 2) metal, immediately after immersion in the aggressive electrolyte. The OCP (E_{oc}) was recorded over 1000 s. Panels (a) of this figure present the potential-time plots of coated and uncoated mild steel, compared with carbon steel (labeled 3 coated and 4 uncoated). The potential-time plots exhibited the same trends; shifting

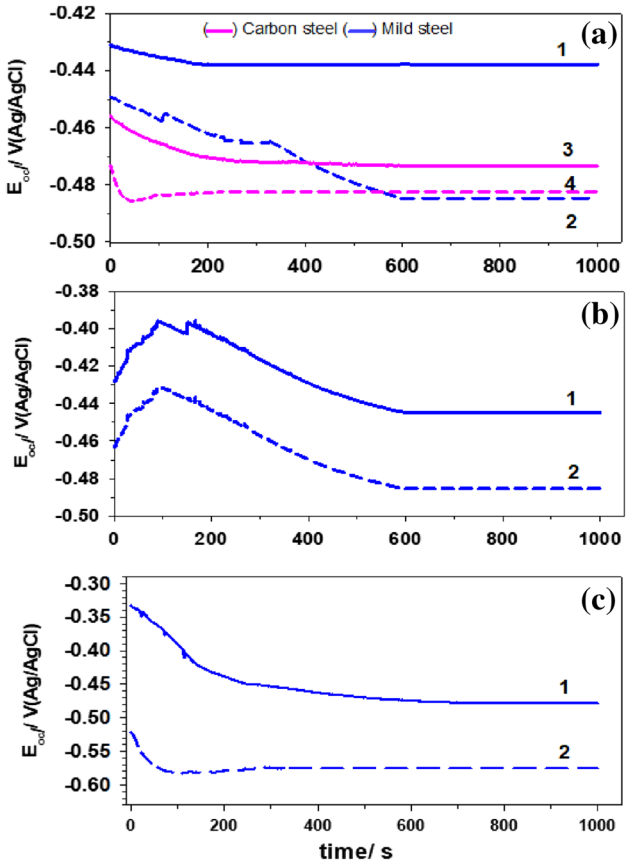

Fig. 5 Variation OCP with time for **a** coated (1, 3) and uncoated (2, 4) mild steel and carbon steel 1 M HCl, **b**, **c** coated (1) and uncoated (2) mild steel in 2 M HCl and 3.5% NaCl, respectively, at 25° C

gradually toward more negative values until reaching the steady-state potential (E_{st}). The steady state was reached in approximately 200 s, except in the uncoated mild steel

which required 600 s. The potential shift to lower negative values indicates that the electrode was stabilized by the formation and deposition of the corrosion layer (iron oxides and hydroxide). As the film of corrosion products built up, it partially covered the microstructure with protective properties. Consequent to the interaction between the steel and aggressive medium (1.0 M HCl), the surface was guarded against further reactions. Figure 5b shows the potential time of coated and uncoated mild steel in 2.0 M HCl aggressive media. E_{oc} shifted to positive values for the first 100 s of immersion, climbing to a clear maximum and then gradually decreasing until a steady-state potential after 600 s. The negative shift can be attributed to the dissolution of the initially grown film. The film was then stabilized by further deposition of the corrosion products. Figure 5C shows the potential time of coated and uncoated mild steel in 3.5% NaCl. The E_{oc} decreased rapidly in the initial phase before reaching a steady-state value at approximately 200 s of immersion. In a steady state, the film formation rate equals the dissolution rate. The final steady value of the electrode potential depended on the Cl^- contents and was much close to the noble phase on the coated surfaces than on the bare steel surfaces.

3.3.2 Electrochemical Impedance Spectroscopy (EIS)

EIS is a popular technique for affirming the properties of the metal surface. EIS shows the frequency-dependent changes in various parameters (i.e., electrode capacitance, charge-transfer resistance, and diffusion resistance). The EIS was measured after the electrodes reached the open circuit potential. Figure 6a displays the Bode and Nyquist plots of mild and carbon steels in 1.0 M HCl. The impedance spectra display resistive regions in the high frequency (HF) and low frequency (LF) ranges, and a marked capacitive response in the middle—frequency range. The impedance spectra show similar features in each case, implying similar corrosion behaviors, but different corrosion rates. The phase maximum of carbon steel in 1 M HCl increased with decreasing impedance |*Z*| with a concomitant shift to a lower frequency; indicating an increase in the double-layer capacitance. The impedance |*Z*| of the coated carbon steel is higher than the uncoated surface. The Nyquist plot of the uncoated carbon steel shows a smaller capacitive loop than of the coated one and also smaller than the uncoated mild steel, but was contrarily upshot indicating that the surface film resistance was reduced by dissolution. However, the coating films prevent the destructive species to penetrate it.

Therefore, the present investigation compares the effects of Cl^- from 1 to 2 M HCl and its salt on uncoated and coated mild steel surface as shown in Fig. 6. Impedance |*Z*| was observed to decrease in 2.0 M HCl while the border phase maximum increased. This trend was attributed to increased adsorption of Cl^- ions on the electrode surface. The Nyquist plot of the coated mild steel in 2 M HCl is characterized by a depressed semicircle at high to medium frequencies with a smaller size than that of uncoated mild steel. Another loop in the lower frequency range separated from the inductive loop indicates that the porous film was affected by the acid concentration and the adsorption of intermediate products. The inductance loop was smaller in uncoated than in coated mild steel in 2 M HCl, indicating that the initial corrosion products were less accumulated on the coated extracts than on the uncoated surface.

The coated mild steel in 1, 2 M HCl generally showed an increased gap phase that can be attributed to increased surface coverage and predominance of the film dissolution process over the formation-modified protection of the coating, and also to the accumulation of corrosion products before the film-healing process. The oxide layer thickness ($1/C$) of the surface film on the coated mild steel was lower than for the uncoated in HCl; indicating the formation of a thicker film at the uncoated surface with a more open structure than the coated surface (which exhibited a thin and compact films). That is to say, the extract coating encourages the growth of a slim layer incorporating the passivating species. The oxide layer thickness (d) was obtained by rearranging the capacitance (formula $C = (\acute{\varepsilon}\, \varepsilon\, A)/\, d$) (see Table 3), where ε is the dielectric constant, $\acute{\varepsilon}$ is the relative permittivity constant of free space (8.85×10^{-12} Fm^{-1}), and A is the exposure area of the working electrode [23].

The Nyquist plots of the electrodes in 1.0, and 2.0 M HCl show a depressed single capacitive semicircle and single maximum phase remote from − 90°. These characteristics indicate a change in the surface roughness, confirming that the electrode processes can be described with one time constant. To model the corrosion process in terms of circuit elements and data analysis, a simple Randles equivalent circuit is a suitable choice [24]. The Randles circuit Fig. 7a includes the electrolyte resistance (R_s) of the solution between the working and the reference electrodes in series with (R_tQ), where R_t represents the total resistance (the charge-transfer resistance and the polarization resistance between the corrosion-product film and solution). These series resistances are connected in parallel with Q, which is considered a constant phase element (*CPE*) rather than an ideal capacitance. The *CPE* accounts for the surface heterogeneity and hence provides a better fit to the data. This model is formulated as $Z_{CPE} = [Y_0\ (j\omega)^{\alpha}]^{-\ 1}$, where Z_{CPE} is the *CPE* impedance ($\Omega\ cm^2$), Y_0 is the admittance constant (Mho), $\omega = 2\pi f$ is the angular frequency (rad s^{-1}), j denotes the imaginary part, and α is an exponential factor ($0 \le \alpha \le 1$) defining the divergence from capacitance linearity; its value is related to the surface roughness [25], 26.

The Nyquist plots of the coated mild steel in HCl show a depressed semicircle with a center below the real axis,

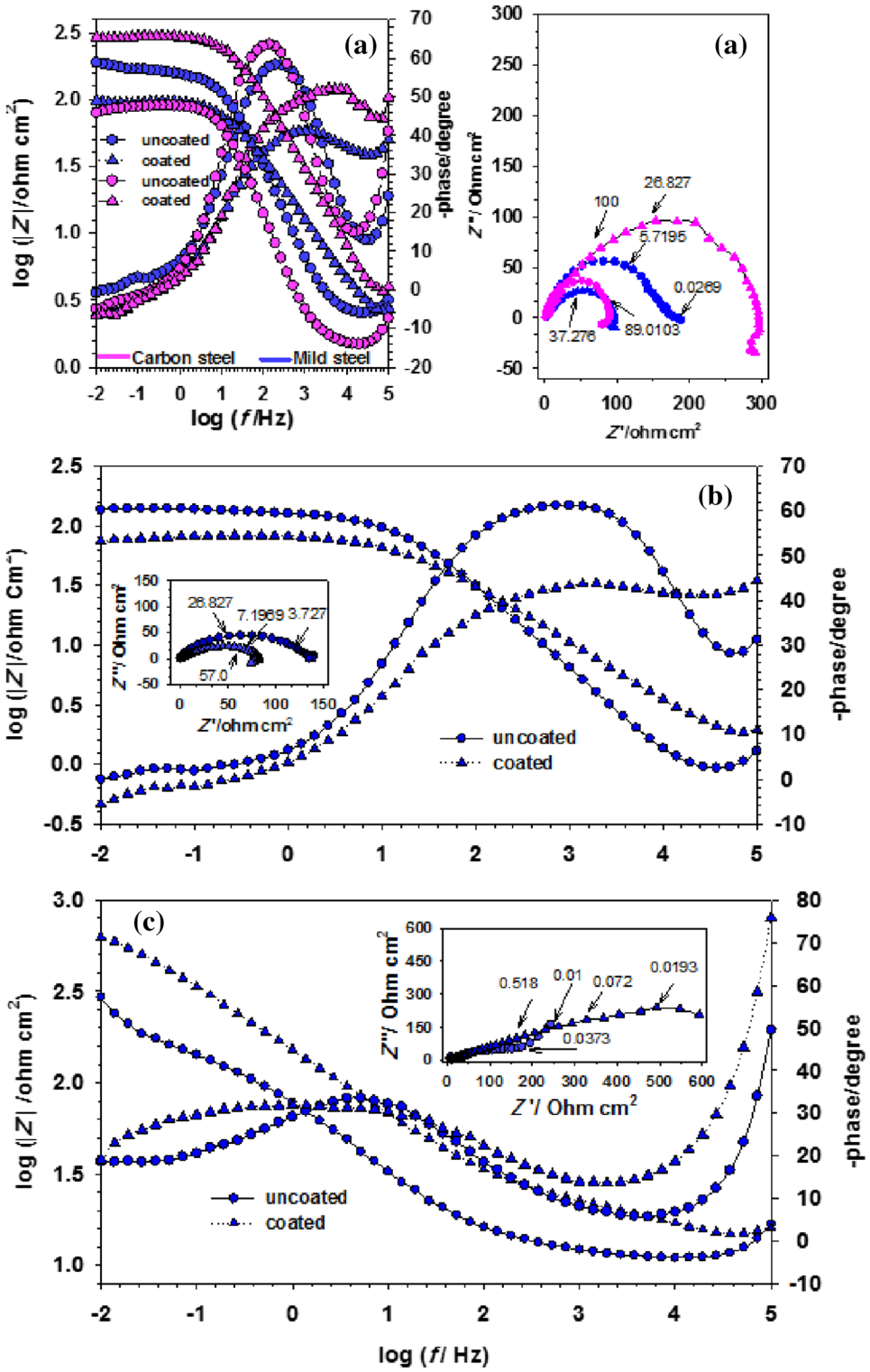

Fig. 6 Electrochemical impedance spectra for **a** coated and uncoated carbon and mild steel in 1 M HCl **b**, **c** coated and uncoated mild steel in 2 M HCl and 3.5% NaCl, respectively, at 25 °C

representing one capacitive loop at HF accompanied by one inductive loop at LF. This behavior typifies an inhomogeneous surface possibly arising from a stabilized by-product layer from the corrosion reaction involving capsaicinoid species and their reactive products. The protection rate depends on the capsaicinoid species and their ability to decrease the number of active sites at the interface of the electrochemical layer formed on the porous film surface in the initial step, as explained later. For analyzing the

Table 3 Fitted impedance parameters for steel in various tested electrolytes derived from impedance measurements

Substrates	Electrolyte	R_t Ω cm^2	Q μF cm^{-2}	α	L μH cm^2	W μF cm^2	R_S Ω cm^2	d μF^{-1} cm^2
Carbon steel								
Uncoated	1 M HCl	58.5	430	0.851	–	–	1.446	0.0023
Coated		203	191	0.628	–	–	1.160	0.0052
Mild steel								
Uncoated	1 M HCl	144.6	166	0.799	–	–	2.400	0.0060
Coated		99.45	572	0.556	345	–	1.245	0.0017
Uncoated	2 M HCl	135.6	219	0.754	–	–	0.660	0.0046
Coated		84.45	610	0.566	256	–	0.630	0.0016
Uncoated	3.5%NaCl	10.315	0.047	0.145	–	0.056	1.920	21.277
Coated		41.85	0.025	0.281	–	0.018	1.785	40.000

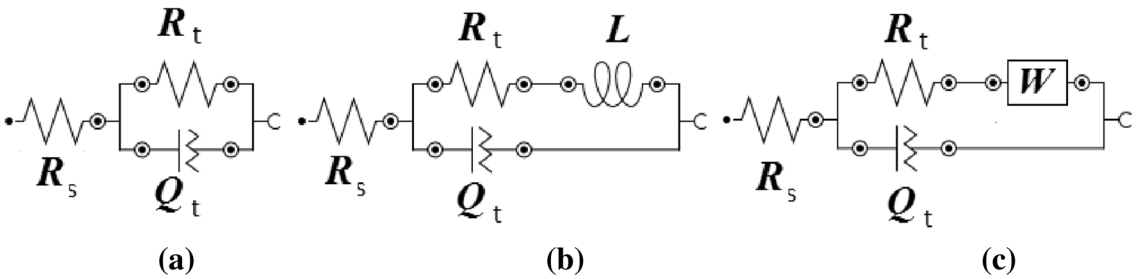

Fig. 7 Equivalent circuit used for simulation of the EIS data: **a** for the uncoated metal in HCl, **b** for the coated metal in HCl, and **c** for the uncoated and coated metal in 3.5%NaCl

data in Fig. 7b, an inductor (L) was added to the simplest circuit, setting $Y = L$ and $\alpha = -1$ [27].

Fig. 6c shows the Bode and Nyquist plots of mild steel in 3.5% NaCl. The salt immersion exerted a profound impact on the impedance |Z|. In particular, the |Z| was largely increased with the increasing value of the phase degree, which gradually shifted to LF. This result indicates continuous passivity with increasing interaction on the electrode surface. The behaviors in the Nyquist plots were confirmed in Bode plots of the impedance responses, which revealed a non-ideal capacitive semicircle with depressed centers near the horizontal axis, followed by a straight line angled at 45° to the abscissa for uncoated mild steel. The diameter of the circuit increased after coating with the slim film, reflecting its effect on the electrode surface [15]. In the Nyquist plot of the coated mild steel, a barely discernible semicircle was followed by a straight line, indicating that resistance was controlled by the charge-transfer process. The straight line indicates that ions were diffused through the modified surface. To model the diffusion of reactants, a Warburg diffusion element (W) was added to the simple equivalent circuit Fig.7c. Here we set $Y = W$ and α =0.5. The Warburg impedance is related to the surface concentration of an electrochemically modified active species [28–30]. Table 3 lists the impedance parameters estimated by the best fitting of the impedance spectra in the aggressive media.

The degree of stability and passivation of the surface films were reflected by the total film resistance under OCP. The surface resistance tended to be lower in uncoated and coated mild steel and higher in HCl owing to increased Cl^- molarity accompanied by reversed Q values. These results illustrate the effect of chloride attack on the corrosion resistance of the surface. In the case of the coated surface, the intensity of the phase-angle signal at 85° in form of the oxide thickness and its adherence. The closed porosity and healed defects in this oxide layer will be demonstrated in the EDX analysis.

Corrosion is an electrochemical process, contributed by individual processes that eventually form an electrolyte layer on the metal. The chloride concentration in 2.0 M and 1.0 M HCl raised the conductivity of the electrolyte film formed on the metal surface and more readily destroyed the initial passivated films than 3.5% NaCl, in which the chloride contents were low. The corrosion rate is a function of the chloride ion activity, which increases with chloride concentration. The phase-angle peak broadening under all criteria confirmed stronger corrosion resistance of the coated mild steel than of the uncoated. As corrosion is a time-dependent phenomenon, the PDP measurements following the EIS

measurements provide the actual kinetics of the electrochemical processes, when all corrosion products remain on the metal surface. The EIS data, which are usually obtained at the OCP, measure the overall interfacial resistance at the electrode–electrolyte interface. They do not estimate the amount of corrosion product.

3.3.3 Potentiodynamic Polarization (PDP)

The corrosion behaviors of the uncoated and coated metals have been measured via potentiodynamic polarization in different corrosive solutions. The potential was scanned from − 1.2 to − 0.5V (vs. Ag/AgCl) at 1.0 mVs^{-1} scan rate. The cathodic and the anodic polarization curves of the uncoated and coated mild steel (Fig. 8a and b, respectively, were obtained in 1.0 M HCl, 2.0 M HCl, and 3.5% NaCl. Fig. 8c displays the curves of coated and uncoated carbon steel in 1.0 M HCl. The slopes of the cathode and anode (βc and βa, respectively) were determined by extrapolating the Tafel straight lines to the corrosion potential. The βc and βa values fluctuated, indicating that the coating extract affected mixed inhibitory responses with a cathodic predominance.

Table 4 summarizes the electrochemical parameters obtained from the polarization curves. The corrosion potential of the uncoated mild steel has a higher negative value of − 546.2, − 476.5, and − 843.5V shifting to the less negative potential for coated surface − 429.70, − 453.00, and − 421.00 in 1 M HCl, 2 M HCl, and 3.5 NaCl, respectively. The more negative potential indicates the reactive surface, consistent with a steadily increasing localized corrosion rate. The current density (i_{corr}) has shifted to lower values from 1.323, 8.290, and 1.185 mA cm^{-2} for uncoated to 0.1962, 0.4388, and 0.0345 mA cm^{-2} for coated mild steel, respectively. This decrease in the corrosion current density expresses the effective protection performance of the extract coating against corrosion

It is evidently seen from the results that the corrosion rate decreases and the resistance increase in the coated metal

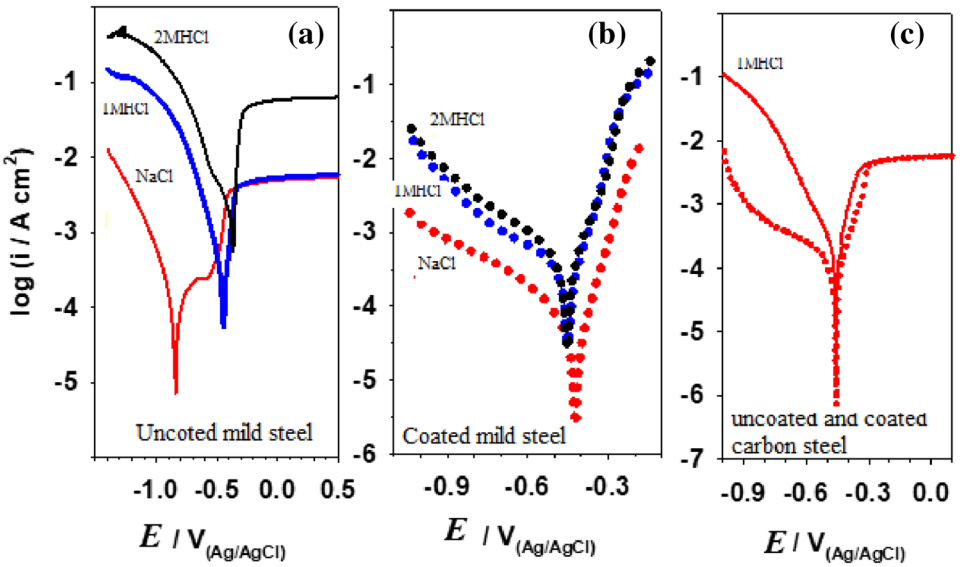

Fig. 8 Potentiodynamic polarization plots **a**, **b** uncoated and coated mild steel in 1,2MHCl and 3.5%NaCl and **c** for coated and uncoated carbon steel in1MHCl at 25 °C

Table 4 Electrochemical corrosion parameters obtained from polarization measurements in various electrolytes

Electrolyte		i_{corr} mA cm^{-2}	*CR* mm y^{-1}	E_{corr} mV	β_a mV dec^{-1}	β_c mV dec^{-1}	R_p Ω cm^2	η%
Carbon steel								
Uncoated	1 M HCl	0.466	5.42	– 479	122.4	129.2	58.57	–
Coated	1 M HCl	0.063	0.73	– 457	170.9	83.7	258.8	86.5
Mild steel								
Uncoated	1 M HCl	1.323	15.38	– 546.2	482.2	202.8	31.2	–
Uncoated	2 M HCl	8.290	64.23	– 476.5	408.0	150.9	5.80	–
Uncoated	3.5% NaCl	1.185	13.77	– 843.5	546.3	-980.8	290.10	–
Coated	1 M HCl	0.196	2.28	– 429.7	77.3	309.6	91.38	85.2
Coated	2 M HCl	0.438	5.09	– 453.0	328.8	147.3	67.15	94.7
Coated	3.5% NaCl	0.034	0.40	– 421.0	195.2	101.6	561.16	97.1

than in the uncoated metal in all aggressive solutions; indicating the increase in corrosion protection

The inhibition efficiency of the coating on mild steel is 85.2% and 94.7% in 1.0 and 2.0 M HCl), however in 3.5% NaCl the inhibition efficiency reached 97.1%. On the other hand, the inhibition efficiency is 86.5% for carbon steel in 1 M HCl. The inhibition efficiency is defined as $\eta = \frac{i_{corr} - i'_{corr}}{i_{corr}} x100$ [14]. Where i_{corr} and i'_{corr}, respectively, denote the corrosion current densities on the uncoated and coated surfaces. The coating of the crispy dry chili extract blocked the active sites on the metal surface and decreased interaction between the steel and aggressive chloride media. Hence the mild steel coated with extract was strongly stable against Cl^- ions; in contrast, the uncoated mild steel was vigorously attacked. Moreover, the steep increase in the corrosion rate corroborates with the EIS results related to relative thickness as seen in Table 3. Uncoated metal with its thick, porous layers were more susceptible to corrosion in aggressive chloride media; their corrosion rates and corrosion current densities were both steeply raised.

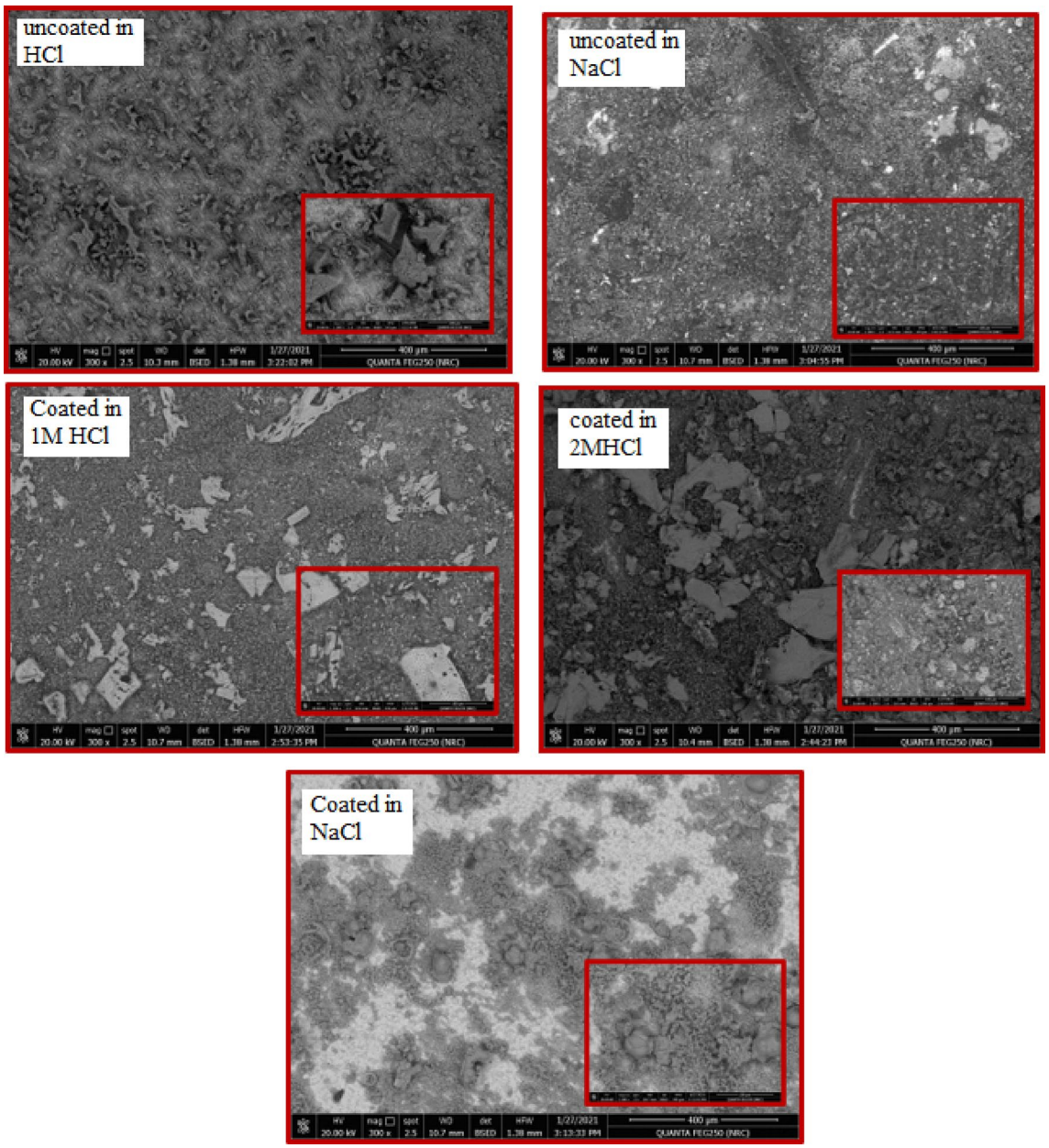

Fig. 9 SEM images for uncoated and coated mild steel in HCl and 3.5% NaCl at 25 °C

3.4 Scanning Electron Microscopy (SEM)

Fig. 9 shows the SEM images of mild steel after immersion in HCl, and 3.5%NaCl without and with a slim capsaicinoids coating collected at room temperature. The images were recorded at the same magnifications for comparison. The chloride anions damaged the surfaces, and the corrosion attack was more pronounced in HCl than in NaCl, owing to the higher dissolution rate. This vicious attack created several lamellar agglomerations which were ascribed to corrosion products. Meanwhile, the oxide layer on the uncoated surface with NaCl created sandy crystals [31]. The inset is a higher-magnification cross-sectional image of uncoated in HCl showing coarse flakes, boxed locations, and multilayered adherences. The interlayer cavities closest to the underlying surface were related to magnetite in the dense and compact, which can peel unevenly [32, 33]. This open structure permitted the easy access of chloride to the substrate as evidenced by the variance between the EIS and PDP results. The surface of the presented grains and flakes were easily peeled. These observations are related to the Cl^- ion activity and the extent of its contribution to the acceleration of metal dissolution as discussed later. The morphologies of the coated mild steel surfaces were smooth surfaces, with compact layers and mounds where the capsaicinoids had interacted with the metal surfaces, protecting them from corrosion. The active species in the coating probably combine with Fe^{2+} ions, forming an insoluble protective layer that strengthens the outermost oxide layer and inhibits the diffusion of Cl^- to the metal surface.

3.5 Computational Studies

The interaction between the metal and capsaicinoids extract coating the surface was numerically investigated by density functional theory calculations (DFT) [34] implemented in Gaussian 16 software [35]. The optimization process and calculations are performed at the B3LYP/6-31 g (d, p) level of theory, which accurately portrays the structural, physical, and chemical properties of C-based nano-systems [36]. Panels (a) and (b) of Fig. 10 show the optimized structures of capsaicin and dihydrocapsaicin, respectively, and panels (c)–(f) show the highest occupied molecular orbital (HOMOs) and lowest unoccupied molecular orbital (LUMOs) of the molecules. The molecular states of the pi-bonds from the benzene ring and the lone electron pair from the O and N atoms on the left side of the molecule have lower energies than the strong sigma bonds on the right side of the molecule. The extended distribution of HOMO cubes on the benzene ring represents the extended C = C pi-bonds and the localized distribution on the N and O- atoms represents their lone pairs. Thus, the capsaicin and dihydrocapsaicin will interact with the metal surface through the O/N lone pairs and the interactive pi-bond electrons.

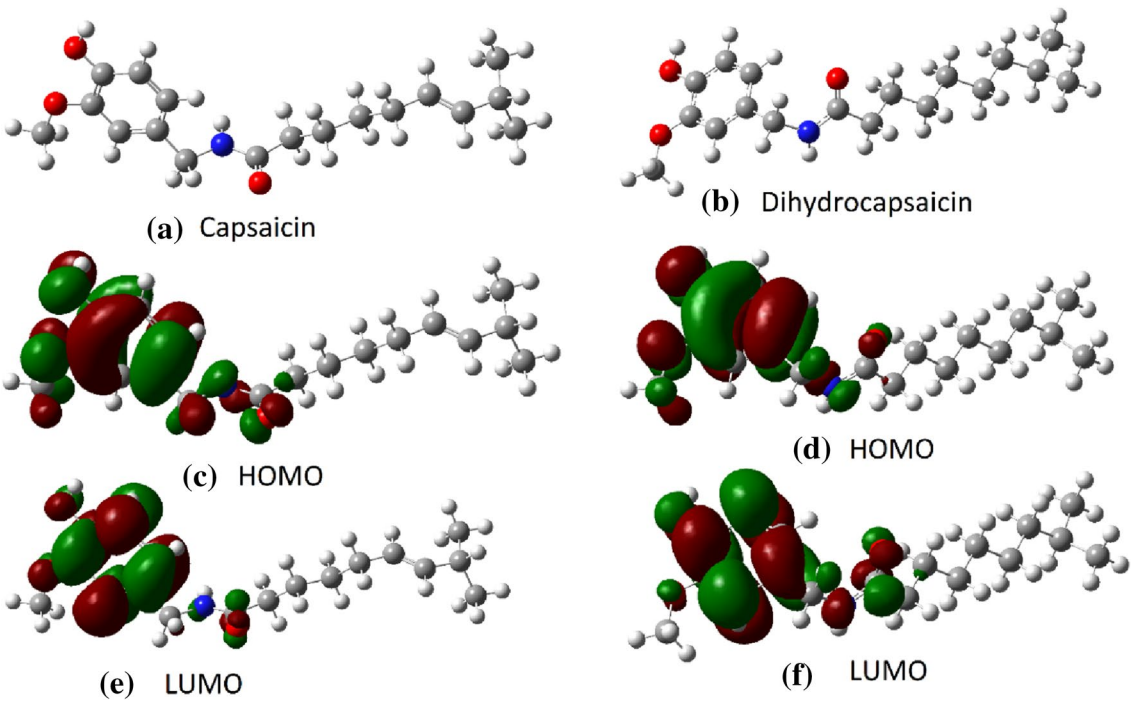

Fig. 10 Optimized structures of capsaicinoids in crispy dry red chilli **a** capsaicin and **b** dihydrocapsaicin with **c**–**f** the corresponding HOMO and LUMO. Atom legend: O red, N blue, C gray, and H white (Color figure online)

Capsaicinoids are phytochemical constituents extracted from capsicum crispy dry chili; they include Capsaicin, dihydrocapsaicin, and nor-dihydrocapsaicin with similar molecular and electronic structures. All constituents process the electronegative heteroatoms N, O, and –OH, and a reactive CH center with fused benzene rings, which can attach to the corroding surfaces of metals [14, 37]. These organic compounds share electrons with the vacant orbital electrons of steel, enabling chemical adsorption through interaction between the lone electrons pairs on the oxygen and nitrogen atoms of the inhibitors and the π bonds of their aromatic rings, which enhance the inhibitor efficiency [38]. The slim coating accumulated at the metal-acid interface prevents further corrosion of the substrate. The experimentally observed corrosion-inhibiting action of the slim coating agreed with the results of quantum chemical calculations, from which the electronic and inhibiting properties of capsaicin and dihydrocapsaicin were calculated. From the HOMO and LUMO energies (E_{HOMO} and E_{LUMO}, respectively), we determined the electronic energy gap(ΔE) = E_{LUMO}-E_{HOMO}, hardness ($\eta = \Delta E/2$), softness ($\sigma = 1/\eta$), and electronegativity ($\chi = (E_{HOMO} + E_{LUMO})/2$) [39].

In additionally, the fraction of transferred electrons between the coated and uncoated metal surfaces was obtained as ΔN (Fe = $(\varphi - \chi_{coated})/(2\ (\eta_{Fe} + \eta_{coated}))$. This indicator well estimates the strength of the interaction between slim coat film and mild steel [40]. Here, φ is the work function of the metal surface, (taken as $\varphi = 4.82$ eV, for the Fe (100) surface) χ_{coated} is the electronegativity of the coated metal, and η_{Fe} and η_{coated} are the hardness values of Fe and the coated mild steel surface, respectively. (Note that $\eta_{Fe} = 0$) because $E_{LUMO} = E_{HOMO}$ in bulk metal). The values of these parameters are given in Table 5. The E_{HOMO} refers to the capability of a molecule to donate electrons to the empty molecular orbitals of an acceptor. When the E_{HOMO} is high, electrons are easily donated to the metal surface. Oppositely, E_{LUMO} refers to the tendency of a molecule to accept electrons. When the E_{LUMO} is high, the molecules are susceptible to nucleophilic attack to accommodate electrons from the surface of the metal. As capsaicin and dihydrocapsaicin have comparable E_{HOMOs} and E_{LUMOs}, their inhibition properties are similar.

The relatively high energy gaps of the selected molecules (5.64 and 5.66 eV in capsaicin and dihydrocapsaicin, respectively) provide an electrically insulating effect that prevents corrosion. Other important parameters are the global hardness η and the global softness σ, which measure the stability and reactivity of the selected molecules. Capsaicin and dihydrocapsaicin are soft molecules with the high softness ($\sigma \sim 0.35$) and low hardness ($\eta = 2.8$) [41] (see Table 5). As the metal undergoes soft–soft interactions with the inhibitor, the evaluated capsaicinoid molecules are considered to be effective corrosion inhibitors [42]. The ΔN values are positive, indicating that the electrons transfer from the inhibitor to the metal surface (the vice-versa behavior occurs for negative ΔN). Accordingly, the inhibitors can donate electrons to the vacant d- orbitals of the metal, eventually passivating them and preventing corrosion.

To study the active sites of the interaction between the inhibitors and the metal surface, we plotted the Mullikan charge distributions and the electrostatic potential contour (ESPs) of capsaicin Fig. 11a and c, respectively) and dihydrocapsaicin, Fig. 11b and d, respectively). In general, inhibitors are adsorbed on metal surfaces through donor–acceptor interactions, which favor highly negatively charged atoms with promising active sites. As shown in Fig. 11a, b, the highly negatively charged atoms in the inhibitors are the O and N atoms and the highly positively charged atoms are their attached C-atoms. Therefore, The O and N atoms represent the active sites of the electrophilic attack. While their neighboring C-atoms represent the active sites of nucleophilic attack. The total dipole (moments μ) of the inhibitors is ~ 3 (*D*) Fig. 11a, b, confirming the high interactivity of the selected molecules. From the ESPs, we can determine the interactive charge-transfer sites and the nucleophilic and electrophilic active sites of the molecule. In an ESP map, the extremely negatively and positively charged atoms are colored red and blue, respectively, and intermediately charged atoms are colored, orange, yellow and green. The ESP contours in Fig. 11c, d support the results of the charge distribution O and N atoms are negatively charged (red and yellow) and their neighboring C-atoms are positively charged blue). Therefore, capsaicin and dihydrocapsaicin contain active sites for both nucleophilic and electrophilic interactions with the metal surface, and so are promising candidates as corrosion inhibitors.

3.6 Inhibition Mechanism

The slim coating shields the surface of the mild steel from chloride attack, reducing the diffusion rate of the chloride ions and changing the anodic or cathodic reactions [43]. In the aggressive medium, the corrosion of the substrates depended on the.

The anodic oxidation, Eq. (1), and cathodic reduction, Eqs. (2), (3)

Table 5 The quantum chemical parameters for the investigated inhibitor

Structure	E_{HOMO} (eV)	E_{LUMO} (eV)	ΔE (eV)	η (eV)	Σ (eV^{-1})	χ (eV)	ΔN
Capsaicin	− 5.5116	0.1303	5.6419	2.8209	0.3545	2.6906	0.3774
Dihydrocapsaicin	− 5.4520	0.2158	5.6678	2.8339	0.3529	2.6181	0.3885

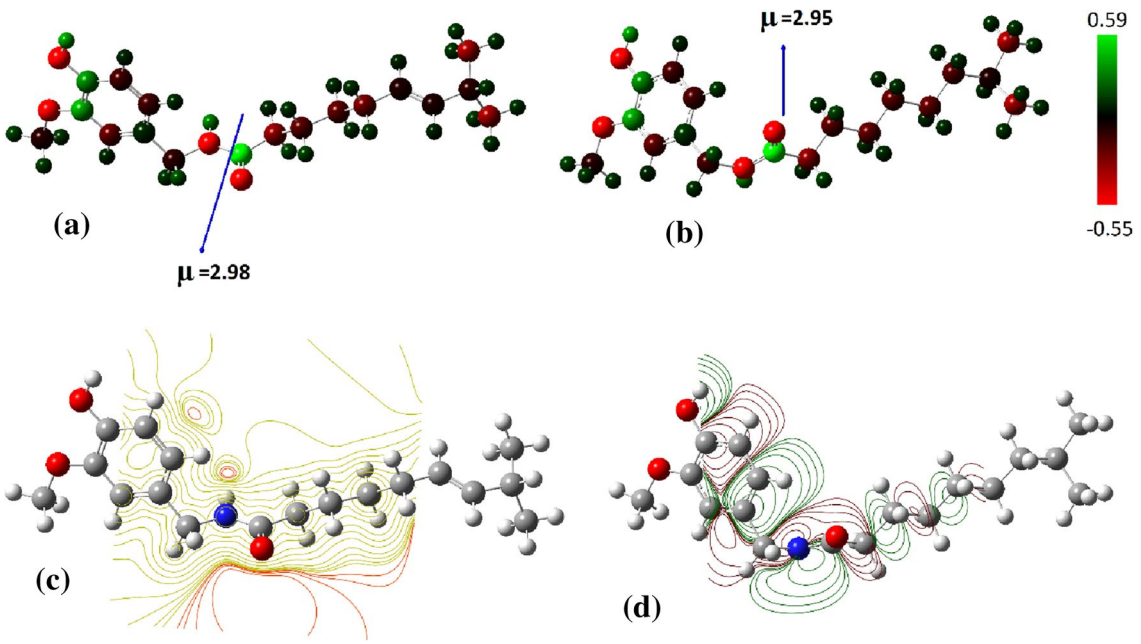

Fig. 11 Charge distribution on capsaicin and dihydrocapsaicin atoms as (**a**, **b**), respectively, and their electrostatic potentials as (**c**, **d**)

$$\text{Fe (solid)} \rightarrow \text{Fe}^{2+} + 2e \quad (1)$$

$$2H^{+} + 2e \rightarrow H_2(g) \quad (2)$$

$$O_2 + 4H^{+} + 4e \rightarrow 2H_2O \quad (3)$$

At the higher acidic, the corrosion process is accelerated, and the surface is severely deteriorated, raising the ionizing chloride, concentration and forming ferrous chloride. The ferrous chloride hydrolyzes as

$$FeCl_2 + H_2O \rightarrow FeO + 2HCl \quad (4)$$

The Cl^{-} in NaCl reacts with $Fe^{2+}$and Fe^{3+} producing the intermediate compounds $FeCl_2$ and $FeCl_3$, respectively. These compounds react with water, forming highly soluble iron hydroxide compounds along with hydrochloric acid:

$$FeCl_2 + 2H_2O \rightarrow Fe(OH)_2 + 2HCl \quad (5)$$

$$FeCl_3 + 3H_2O \rightarrow Fe(OH)_3 + 3HCl \quad (6)$$

These corrosion products create a thick gel [FeO (OH)] that can react with iron cations to form a passive film of magnetite which is easily deteriorated by Cl^{-} attack [44], and with the diffusion of aggressive species from the media:

$$8\,FeOOH + Fe^{2+} + 2e^{-} \rightarrow 3Fe_3O_4 + 4H_2O \quad (7)$$

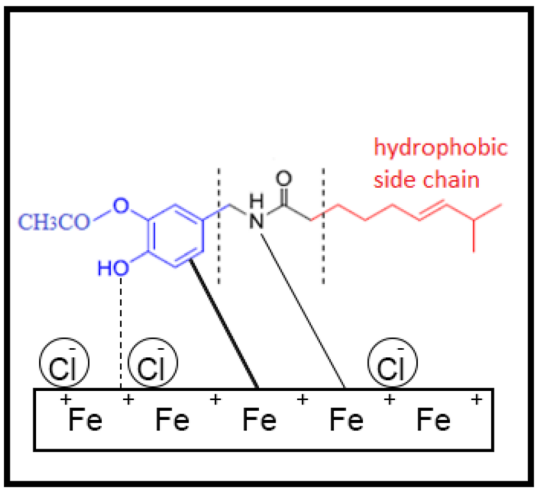

Fig. 12 Proposed mechanism of the adsorption behavior of Capsaicinoid on mild steel surface

The corrosion protection effectiveness of capsaicinoids (active materials in the coating) in different aggressive media can be attributed to electrochemical oxidation or reduction. In aggressive solutions, capsaicinoids (with chemical formula $C_{18}H_{27}NO_3$) undergo an irreversible anodic oxidation reaction with the discard of two electrons, forming a 2-methoxy group and H^{+}. After hydrolysis with the loss of the proton and methanol, o- benzoquinone is formed, which is reduced to o- hydroxy-phenol [15].

Furthermore, the capsaicinoid molecules (heteroatom of oxygen and nitrogen) were expected to cause an easier electron transfer to the steel surface; hence, greater adsorption ability was obtained as shown in Fig. 12. It was found that the adsorbed molecules remain stable on the steel surface, even after being immersed in aggressive media. In general, the adsorbed capsaicinoids impede corrosion by simply blocking the reaction sites on the surface, thus inhibiting the oxygen and hydrogen evolution reaction.

4 Conclusion

During long-term (5 days) immersion in aggressive media, the corrosion of steel coated with a thin film of capsaicinoids was controlled by ion transport. In 3.5% NaCl, the corrosion products were non-cohesive, and the inhibitions efficiency of the coating reached 97.1%. In HCl, the corrosion process depended on the oxide layer linked to Cl^- concentrations, and the corrosion process was more severe and led to a cracked surface. The capsaicinoids extract improved the electrochemical stability of the formed anodic layer, conferring superior corrosion resistance and a stable surface. On mild steel, the inhibition efficiencies reached 94.7% and 85.2% in the presence of 2.0 M HCl and 1.0 M HCl, respectively. Quantum chemical and theoretical studies proved that extract was the electron donor to the steel surface.

Acknowledgements Authors would like to thank (APOTECBAY), Egypt for its support.

Funding This research did not receive any specific grant from funding agencies in the public, commercial, or not-for-profit sectors.

Data Availability All data generated or analyzed during this study are included in this published article, data will be available on reasonable request.

Declarations

Conflict of interest The authors declare no conflict of interest.

References

1. Rani BEA, Basu BBJ (2012) Green inhibitors for corrosion protection of metals and alloys: an overview. Int J Corros 2012:380217. https://doi.org/10.1155/2012/380217
2. Abou-Elseoud WS, Abdel-karim AM, Hassan EA, Hassan ML (2021) Enzyme-and acid-extracted sugar beet pectin as green corrosion inhibitors for mild steel in hydrochloric acid solution. Carbohydr Polym Technol Appl 2:100072
3. Abdel Hameed R, Essa A, Mohamed D, Abdallah M, Aljohani M, Al-Mhyawi S, Soluman M, Arafa EI (2022) Evaluation of expired augmentine drugs as corrosion inhiitor for carbon steel alloy in 1.0 n hcl acidic environment using analytical techniques. Egypt J Chem 65:1–2
4. Abdel Hameed RS, Al-Bagawi AH, Shehata HA, Shamroukh AH, Abdallah M (2020) Corrosion inhibition and adsorption properties of some heterocyclic derivatives on C-steel surface in HCl. J Bio Tribo-Corros 6:1–11
5. Hameed A, Alfakeer M, Abdallah M (2018) Inhibiting properties of some heterocyclic amide derivatives as potential nontoxic corrosion inhibitors for carbon steel in 1.0 M sulfuric acid. Surf Eng Appl Electrochem 54:599–606
6. Shahen S, Abdel-Karim AM, Gaber GA (2021) Eco-friendly roselle (*Hibiscus Sabdariffa*) leaf extract as naturally corrosion inhibitor for Cu-Zn alloy in 1M HNO3. Egypt J Chem. https://doi.org/10.21608/ejchem.2021.92917.4392
7. Oki M, Ebitei C, Alaka C, Oki TK (2011) Corrosion inhibition of mild steel in hydrochloric acid by tannins from *Rhizophora racemosa*. Mater Sci Appl 2:592–595
8. Abdel-Karim AM, El-Shamy AM (2022) A review on green corrosion inhibitors for protection of archeological metal artifacts. J Bio Tribo-Corros 8:1–21
9. Reddy CM, Sanketi BD, Narendra Kumar S (2016) Corrosion inhibition of mild steel by *Capsicum annuum* fruit paste. Perspect Sci 8:603–605. https://doi.org/10.1016/j.pisc.2016.06.033
10. Walpole CSJ, Wrigglesworth R, Bevan S, Campbell EA, Dray A, James IF, Perkins MN, Reid DJ, Winter J (1993) Analogs of capsaicin with agonist activity as novel analgesic agents; structure-activity studies. 1. The aromatic "A-region." J Med Chem 36:2362–2372. https://doi.org/10.1021/jm00068a014
11. Walpole CSJ, Wrigglesworth R, Bevan S, Campbell EA, Dray A, James IF, Masdin KJ, Perkins MN, Winter J (1993) Analogs of capsaicin with agonist activity as novel analgesic agents; structure-activity studies. 2. The amide bond "B-region." J Med Chem 36:2373–2380. https://doi.org/10.1021/jm00068a015
12. Walpole CSJ, Wrigglesworth R, Bevan S, Campbell EA, Dray A, James IF, Masdin KJ, Perkins MN, Winter J (1993) Analogs of capsaicin with agonist activity as novel analgesic agents; structure-activity studies. 3. The hydrophobic side-chain "C-region." J Med Chem 36:2381–2389. https://doi.org/10.1021/jm00068a016
13. Kurniawan F, Madurani K (2015) Electrochemical and optical microscopy study of red pepper seed oil corrosion inhibition by self-assembled monolayers (SAM) on 304 SS. Prog Org Coat 88:256–262. https://doi.org/10.1016/j.porgcoat.2015.07.010
14. Prakash R (2012) Green Capsicum annuum fruit extract for inhibition of mild steel corrosion in hydrochloric acid solution. Int J Electrochem Sci 7:12146–12158
15. Vaszilcsin C, Dan M, Enache AF, Hulka I (2016) Inhibiting corrosion process of carbon steel in sodium chloride aqueous solution by capsaicin extract. Chem. Bull. 61(75):1
16. Sun X, Yu L (2018) Investigation of polyacrylamide containing capsaicin monomer as a novel corrosion inhibitor for mild steel in hydrochloric acid. Mater Corros 69:1095–1103. https://doi.org/10.1002/maco.201709876
17. Zhou J, Zhang X, Yan Y, Hu J, Wang H, Cai Y, Qu J (2019) Preparation and characterization of a novel antibacterial acrylate polymer composite modified with capsaicin. Chin J Chem Eng 27:3043–3052. https://doi.org/10.1016/j.cjche.2019.03.024
18. Belaud V, Valette S, Stremsdoerfer G, Bigerelle M, Benayoun S (2015) Wettability versus roughness: multi-scales approach. Tribol Int 82:343–349. https://doi.org/10.1016/j.triboint.2014.07.002
19. Suica-Bunghez I-R, Ion R-M (2020) Characterization, phytochemical and antioxidant activity of three types of hot pepper (*Capsicum annuum* L.). J Sci Arts 20:443–450
20. Zhou J, Zhang X, Yan Y, Jianfeng Hu, HangWang YC, Qu J (2019) Preparation and characterization of a novel antibacterial

acrylate polymer composite modified with capsaicinoids. Chin J Chem Eng 27:3043–3052
21. El-Kaaby E, Al Hattab Z (2016) FT-IR Identification of capsaicin from callus and seedling of chilli pepper plants *Capsicum annuum* L. in vitro. Intl J Multidiscip Curr Res 4:1144–1146
22. Rajendran S, Apparao BV, Palaniswamy N, Periasamy V, Karthikeyan G (2001) Corrosion inhibition by strainless complexes. Corros Sci 43:1345–1354
23. Machuca LL, Lepkova K, Petroski A (2017) Corrosion of carbon steel in the presence of oilfield deposit and thiosulphate-reducing bacteria in CO2 environment. Corros Sci 129:16–25. https://doi.org/10.1016/j.corsci.2017.09.011
24. Oguzie EE, Wang SG, Li Y, Wang FH (2009) Influence of iron microstructure on corrosion inhibitor performance in acidic media. J Phys Chem C 113:8420–8429. https://doi.org/10.1021/jp9015257
25. El-Haddad MAM, Bahgat Radwan A, Sliem MH, Hassan WMI, Abdullah AM (2019) Highly efficient eco-friendly corrosion inhibitor for mild steel in 5 M HCl at elevated temperatures: experimental & molecular dynamics study. Sci Rep 9:3695. https://doi.org/10.1038/s41598-019-40149-w
26. Mandour HS, Abdel-Karim AM, Fathi AM (2021) Inhibition efficiency of copper corrosion in a neutral chloride solution by barbituric and thiobarbituric acids. Port Electrochim Acta 39:85–103
27. Singh A, Lin Y, Quraishi M, Olasunkanmi L, Fayemi O, Sasikumar Y, Ramaganthan B, Bahadur I, Obot I, Adekunle A, Kabanda M, Ebenso E (2015) Porphyrins as corrosion inhibitors for N80 steel in 3.5% NaCl solution: electrochemical, quantum chemical, QSAR and monte carlo simulations studies. Molecules 20:15122–15146. https://doi.org/10.3390/molecules200815122
28. Fasmin F, Srinivasan R (2015) Detection of nonlinearities in electrochemical impedance spectra by Kramers-Kronig Transforms. J Solid State Electrochem 19:1833–1847. https://doi.org/10.1007/s10008-015-2824-9
29. Popova A, Raicheva S, Sokolova E, Christov M (1996) Frequency dispersion of the interfacial impedance at mild steel corrosion in acid media in the presence of benzimidazole derivatives. Langmuir 12:2083–2089. https://doi.org/10.1021/la950148+
30. Yadav M, Kumar S, Bahadur I, Ramjugernath D (2014) Electrochemical and quantum chemical studies on synthesized phenylazopyrimidone dyes as corrosion inhibitors for mild steel in a 15% HCl solution. Int J Electrochem Sci 9:3928–3950
31. Dhaiveegan P, Elangovan N, Nishimura T, Rajendran N (2016) Weathering steel in industrial-marine-urban environment: field study. Mater Trans 57:148–155. https://doi.org/10.2320/matertrans.M2015345
32. Raman A, Nasrafadani S, Sharma L, Rafvan A (1987) Morphology of rust phases formed on weathering steels during outdoor atmospheric exposure in open bold locations. Prakt Metallogr 24:577–589
33. Patni N, Agarwal S, Shah P (2013) Greener approach towards corrosion inhibition. Chin J Eng 2013:784186. https://doi.org/10.1155/2013/784186
34. Hohenberg P, Kohn W (1964) Inhomogeneous electron gas. Phys Rev 136:B864
35. Frisch MJ, Trucks GW, Schlegel HB, Scuseria GE, Robb MA, Cheeseman JR, Scalmani G, Barone V, Petersson GA, Nakatsuji H, Li X, Caricato M, Marenich AV, Bloino J, Janesko BG, Gomperts R, Mennucci B, Hratchian HP, Fox DJ (2016) Gaussian 16 Rev. C.01. Wallingford, CT
36. Abdelsalam H, Saroka VA, Younis WO (2021) Corrigendum to "Edge functionalization of finite graphene nanoribbon superlattices" [Superlattice. Microst. 129, (2019) 54–61]. Superlattices Microstruct 154:106887. https://doi.org/10.1016/j.spmi.2021.106887
37. Harborne A (1998) Phytochemical methods a guide to modern techniques of plant analysis. Springer science & business media, Berlin
38. Shahen S, Gaber G (2021) 4-Aminobenzenesulfonic acid as effective corrosion Inhibitor for carbon steel in hydrochloric acid. Egypt J Chem 64:825–834
39. Cao Z, Tang Y, Cang H, Xu J, Lu G, Jing W (2014) Novel benzimidazole derivatives as corrosion inhibitors of mild steel in the acidic media. Part II: Theoretical studies. Corros Sci 83:292–298
40. El-Hajjaji F, Ech-chihbi E, Rezki N, Benhiba F, Taleb M, Chauhan DS, Quraishi MA (2020) Electrochemical and theoretical insights on the adsorption and corrosion inhibition of novel pyridinium-derived ionic liquids for mild steel in 1 M HCl. J Mol Liq 314:113737. https://doi.org/10.1016/j.molliq.2020.113737
41. Ech-chihbi E, Nahlé A, Salim R, Oudda H, El Hajjaji F, El Kalai F, El Aatiaoui A, Taleb M (2019) An investigation into quantum chemistry and experimental evaluation of imidazopyridine derivatives as corrosion inhibitors for c-steel in acidic media. J Bio Tribo-Corros 5:24. https://doi.org/10.1007/s40735-019-0217-9
42. Saha SK, Banerjee P (2015) A theoretical approach to understand the inhibition mechanism of steel corrosion with two aminobenzonitrile inhibitors. RSC Adv 5:71120–71130. https://doi.org/10.1039/C5RA15173B
43. Kaesche H (2003) Rusting of iron and steel. Springer, Berlin, pp 193–203
44. Harbone JD (1998) Phytochemical Methods. Springer, Berlin